Frequency Multiplexing of Remote All-Fiber Michelson Interferometers With Lead Insensitivity

J. L. Santos, F. Farahi, T. Newson, A. P. Leite, and D. A. Jackson

Abstract— **A scheme to frequency multiplex a group of sensors based on all-fiber Michelson interferometers is presented. Lead insensitivity is obtained by using the two fibre leads of the configuration as an extra Michelson interferometer whose differential phase is kept constant by active compensation. Topics concerning the system design, sensor sensitivity, and crosstalk between sensors are investigated. Experimental and numerical computational results are presented.**

I. Introduction

FIBER-OPTIC interferometric sensors have been actively studied and developed using different optical configurations and signal processing techniques [1]. For applications where arrays of sensors are needed, multiplexing of fiber sensors will result in significant cost savings due to reduction in the number of light sources, detectors and fibre transmission lines required. A number of different approaches to sensor multiplexing have been reported, which may be described as forms of coherence, frequency and time division multiplexing [2], [3]. For all of these techniques it is desirable that the sensor heads should be as simple as possible, without electrical connections, and that phase/intensity fluctuations induced in the lead fiber(s) due to environmental disturbances should not substantially degrade the system performance. Several schemes have been proposed to remove the environmental disturbance generated in the transceiver fiber link [4]–[6]. Here, we present a scheme to multiplex a group of sensors, based on all fiber Michelson interferometers, in which the problem of lead sensitivity is solved by using active compensation. The concept is illustrated in Fig. 1. The two arms of the Michelson interferometers can either be located remotely from the source, detector and processing electronics, or, alternatively, only the signal arms are located remotely, while the reference arms are located in a controlled environment in the processing region (dotted box in Fig. 1). In order to overcome the problem of lead sensitivity, the fibers that guide light to the arms of the sensing Michelson interferometers form an additional

Manuscript received February 7, 1991.

J. L. Santos and A. P. Leite are with the Physics Laboratory U. Porto/INESC Porto, P. Gomes Teixeira, 4000 Porto, Portugal/L. Mompilher 22,4000 Porto, Portugal.

F. Farahi was with the Applied Optics Group, Physics Laboratory U. Kent, Canterbury, Kent, CT27NR, UK. He is now with the Physics Department, The University of North Carolina & Charlotte at Charlotte, NC 28223.

T. Newson was with the Applied Optics Group, Physics Laboratory U. Kent, Canterbury, Kent, CT27NR, UK. He is now with the Department of Electronics and Computer Science, U. Southampton, Southampton, Hants S09, 5NH, UK.

D. A. Jackson is with the Applied Optics Group, Physics Laboratory U. Kent, Canterbury, Kent, CT27NR, UK.

IEEE Log Number 9107683.

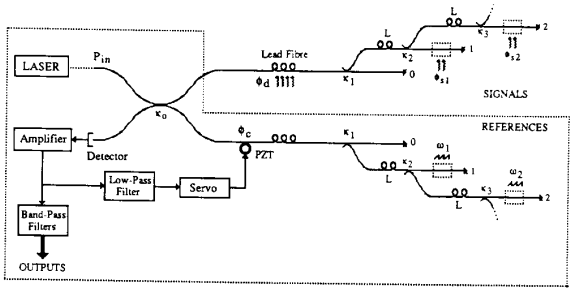

Fig. 1. Scheme to frequency multiplex a group of all fiber Michelson interferometers with lead insensitivity.

Michelson interferometer, whose differential phase is kept constant by a servo system fed by the amplifier output after low-pass filtering. Light from each interferometer is made incoherent with respect to light from other interferometers by introducing portions of fiber with length L greater than the source coherence length. To recover the signals, a carrier of frequency "ω_j" ($j = 1, 2, \cdots, N$, where N is the number of sensors) is generated for the jth interferometer by one of two methods: 1) ramping the injection current of the laser diode (and hence the frequency of the emitted radiation) in combination with a unique path imbalance for each interferometer; 2) applying a ramp voltage to a PZT located in the reference arm of each sensing interferometer. At the output, the interferometers carriers are separated using a set of bandpass filters.

II. Theory

A. System Design

The criterion to determine the coupling ratios of the directional couplers is to ensure that each interferometer (including the compensating interferometer) contributes the same average power to the detector, and that each arm of an individual interferometer receives the same power level. This last condition implies the symmetry of the design, so that the coupling ratios of corresponding couplers in the sensing and reference branches are the same. Two cases can be considered:

1) Lossless System: The average power on the detector from the ith interferometer is

$$P_i = 2P_{\text{in}}\kappa_o(1-\kappa_o)(1-\kappa_{i+1})^2\prod_{j=1}^{i}\kappa_j^2; \quad (i = 1, 2, \cdots, N) \tag{1}$$

where "P_{in}" is the injected power and "κ_j" is the coupling ratio of the jth interferometer. The average power returned from the 0–th interferometer—the compensating interferometer—is $2P_{\text{in}}\kappa_o(1-\kappa_o)(1-\kappa_1)^2$. The condition $P_{i+1} = P_i$ gives the relation

$$\kappa_{i+1} = 2 - \frac{1}{\kappa_i}. \tag{2}$$

As $\kappa_{N=1} = 0$, we have

$$\kappa_i = \frac{N+1-i}{N+2-i} \qquad (i = 1, 2, \cdots, N). \tag{3}$$

With the couplers splitting ratios constrained in this way, the average power returned from each interferometer is

$$P_{\text{int}} = \frac{2P_{\text{in}}\kappa_o(1-\kappa_o)}{(N+1)^2} \tag{4}$$

where "$N+1$" is the number of interferometers; the total returned average power is $P_t = (N+1)P_{int}$

2) Real System: The analysis is simplified if it is assumed that losses in fibers, splices, couplers, etc., are lumped together in the couplers, giving a power attenuation factor of 1-β each time the light crosses a coupler. From Fig. 1 it can be seen that 1-β is approximately equal to the total loss in a fiber length L. in one coupler and three fusion splices. With this model, we have ($\kappa_N = 1/2, \kappa_{N+1} = 0$),

$$\kappa_i = 1 - \frac{1-\kappa_{i-1}}{\beta\kappa_{i-1}}; \qquad (i = 1, 2, \cdots, N-1) \tag{5a}$$

$$\kappa_i = \frac{\sum_{j=i}^{N-1} \beta^{(N-1)-j} + 1}{\sum_{j=i}^{N} \beta^{(N-j)} + 1} \qquad (i = 1, 2, 3 \cdots, N-1) \tag{5b}$$

$$P_{\text{int}} = 2P_{\text{in}}\kappa_o(1-\kappa_o)\frac{\beta^{2(N+1)}}{\left[\sum_{j=1}^{N} \beta^{(N-j)} + 1\right]^2};$$

$$P_t = (N+1)P_{\text{int}}. \tag{5c}$$

To maximize the power that reaches the detector, "κ_o" must be 0.5 in (4) and (5c). Fig. 2 shows the variation of "P_{int}" (normalized by the input power) with the number of sensors, for a lossless and a lossy system ($\beta = 0.9$, which means a lumped loss of 0.5 dB).

B. Sensor Sensitivity

In this section, the minimum detectable phase signal from the sensors in the system is evaluated, considering the primary noise sources (namely, phase noise, shot noise, and electronic noise). It is assumed that the coupling ratios of the couplers follow the relations given in Section II-A, which ensure that all sensors return the same average power.

In the frequency range of interest for sensor applications the (one-sided) phase noise power spectral density at the output of a two beam interferometer with differential delay "τ"

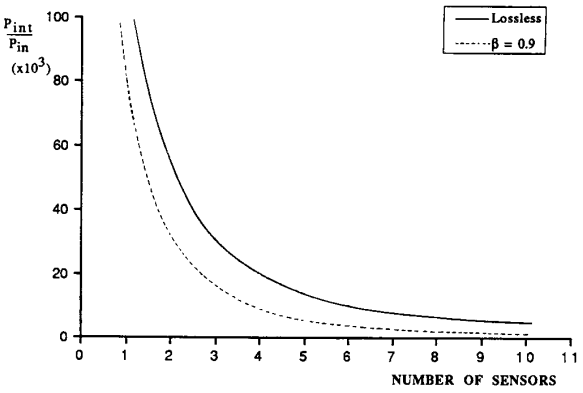

Fig. 2. Returned average power from each sensing interferometer (normalized by the input power) for lossless and lossy ($\beta = 0.9$) systems.

illuminated by a source with coherence time "τ_c" (assuming negligible intensity noise and phase fluctuations of the light that follow a Gaussian probability distribution) is given by [7]

$$G_{\text{PhaseNoise}} \approx 8P_AP_B\tau_c e^{-\frac{2\tau}{\tau_c}}\left\{\sin^2(\omega_o\tau)\left[\cosh\left(\frac{2\tau}{\tau_e}\right) - 1\right] + \cos^2(\omega_o\tau)\left[\sinh\left(\frac{2\tau}{\tau_c}\right) - \frac{2\tau}{\tau_c}\right]\right\} \tag{6}$$

where "P_A", "P_B" are the optical powers that reach the detector from each arm of the interferometer ($P_A = P_B = P_{\text{int}}/2$) and $\omega_o = 2\pi v_o$, where "v_o" is the frequency of the optical radiation. In the coherent regime $2\tau/\tau_c << 1$, and (6) can be written

$$G_{\text{PhaseNoise}} \approx 16P_AP_B\frac{\tau^2}{\tau_c}\sin^2(\omega_o\tau); \qquad \left(\frac{2\tau}{\tau_c} << 1\right). \tag{7}$$

In the incoherent regime $2\tau/\tau_c >> 1$ and (6) becomes

$$G_{\text{PhaseNoise}} \approx 4P_AP_B\tau_c; \qquad \left(\frac{2\tau}{\tau_c} >> 1\right). \tag{8}$$

For the topology shown in Fig. 1 the number of paths from the source to the detector is $2(N+1)$. The number of pairs of paths is

$$^{2(N+1)}C_2 = (2N+1)(N+1). \tag{9}$$

For "$N+1$" of these pairs the condition $2\tau/\tau_c << 1$ is satisfied and (7) is valid. For the pair that constitutes the jth interferometer ($j = 1, 2, \cdots, N$)

$$\sin(\omega_o\tau) = \sin[\omega_j t + \phi_{oj} + \phi_{sj}\sin(\omega_{sj}t)] \tag{10}$$

where "$\phi_{sj}\sin(\omega_{sj}t)$" is the applied signal, $\phi_{oj} = 2\pi n v_o \Delta L_j/c$ is the static phase difference and "ω_j" is the carrier frequency generated by the pseudo-heterodyne technique ("ΔL_j" is the geometric path imbalance of the jth interferometer, "c" is the speed of light and "n" is the effective index of the fiber mode). If $\phi_{sj} << 1$, this pair contributes to

the level of phase noise at frequencies $\omega_j \pm \omega_s$ by the amount $4P_AP_B(\tau^2\phi_s^2/\tau_c)$, which is negligible. On the other hand, the other "N" pairs that constitute the remaining "N" sensing interferometers do not introduce phase noise at frequencies $\omega_j \pm \omega_s$ (because it is assumed that each sensing interferometer has a different carrier frequency). Therefore, the level of phase noise arises from the ${}^{2(N+1)}C_2 - (N+1)$ pairs which are described by (8), i.e.,

$$G_{\text{PhaseNoise}} \approx 4[(2N+1)(N+1) - (N+1)]P_AP_BM^2\tau_c = 8N(N+1)P_AP_BM^2\tau_c \quad (11)$$

where "M", the detector current multiplication gain obtained when an APD is used, is modeled in terms of an equivalent predetection optical amplification.

Expression (11) was obtained by adding the spectral noise powers of the interferometers which fulfill the condition $2\tau/\tau_c >> 1$. Therefore, possible correlations of phase noise powers associated with two or more interferometers were not taken into account. If the path imbalance of each pair of paths was unique in the scale of the source coherence length, or if the average delay for each of those pairs was unique in the scale of the source coherence time, then the correlation would be negligible and phase noise powers will simple add. However, for the configuration shown in Fig. 1, if the length "L" of fiber between adjacent interferometer arms is constant, then there are pairs of paths with average delays and path imbalances which are similar on the scale of the source coherence time or source coherence length, respectively. Therefore, correlations between noise powers of different interferometers may exist which are proportional to "$\cos(\phi_{r2} - \phi_{r1} + \phi_{s2} - \phi_{s1})$", where "$\phi_{r1}$", "$\phi_{r2}$," and "$\phi_{s1}$," "$\phi_{s2}$" are the net phase delays (static and variable) for the light that propagates in the reference and sensing arms of two interferometers which fulfill the conditions for mutual phase noise correlation [8]. Accepting that the fluctuations, as well as the signal and reference phases applied to one of the interferometers, are independent from those applied to the other one, within the frequency range of each sensor the correlation factor will be small and the total phase noise power spectral density will be given approximately by (11).

The shot noise current generated in the detection process is (rms value)

$$i_{\text{shot}} = \sqrt{2eM^2F\mathcal{R}P_tB} \quad (12)$$

where "e" is the electron charge, "F" is the excess noise factor of the detector, "$\mathcal{R}$" is the detector responsivity and "B" is the system bandwidth. It is convenient to express the shot noise current in terms of an equivalent one-sided squared optical noise spectral density, "$G_{\text{ShotNoise}}$", defined by

$$G_{\text{ShotNoise}}(f) = \frac{i_{\text{shot}}^2}{\mathcal{R}^2} = \frac{2P_tM^2Fhv_o}{\eta} \quad (13)$$

where "h" is the Planck constant and "η" is the detector quantum efficiency.

Other noise sources need to be considered, namely the shot noise associated with the dark current "i_{dark}" of the detector, the thermal noise generated in the feedback resistance "R_f" of the transimpedance amplifier and the noise generated in the amplifier itself. Lumping these noise sources together as electronic noise, we have (again, in terms of an equivalent one-sided squared optical noise spectral density)

$$G_{\text{Electronic}} = \left(\frac{hv_o}{\eta e}\right)^2\left[2ei_{\text{dark}}M^2F + \frac{4K\theta}{R_f} + i_n^2\right] \quad (14)$$

where "K" is the Boltzmann constant, "θ" is the absolute temperature, and "i_n" is the noise current of the amplifier.

The output from the jth interferometer is

$$P_j = P_{\text{int}}\{1 + V\cos[\omega_j t + \phi_{oj} + \phi_{sj}\sin(\omega_{sj}t)]\} \quad (15)$$

where "V" is the fringe visibility (for simplicity it will be assumed that the visibility will be the same for all sensing interferometers). If $\phi_{sj} << 1$, the optical rms signal present in any of the two sidebands of "ω_j" is "$(V/\sqrt{8})\phi_{sj}P_{\text{int}}$"; the corresponding squared optical power signal is (with the APD gain modelled in terms of an equivalent predetection optical amplification)

$$S = \frac{V^2}{8}P_{\text{int}}^2M^2\phi_{sj}^2. \quad (16)$$

For SNR= 1, $S = BG_x$, where "x" indicates each one of the noise sources considered above. Therefore, the minimum detectable phase when the noise source "x" is present is

$$\phi_{sx} = \sqrt{\frac{8BG_x}{V^2P_{\text{int}}^2M^2}}. \quad (17)$$

Fig. 3 (a) shows the variation of the minimum detectable phase signal with the number of sensors when only phase noise is considered ($M = F = 1, V = 0.5$, $\tau_c = 1.2 \times 10^{-8}s$ ($L_c = 3.6$ m); the coherence time corresponding to a single-mode laser emitting 3 mW of optical power [9]). Fig. 3 (b) gives the minimum detectable phase as determined by shot noise and electronic noise $v_o = 3.75 \times 10^{14}$ Hz ($\lambda = 800$ nm), $P_{\text{in}} = 1$ mW, $\eta = 0.6$, $V = 0.5$, $i_n = 7 \times 10^{-13}A/\sqrt{\text{Hz}}$ (for the 5534 low noise amplifier), $R_f = 100$ kHz, $i_{\text{dark}} = 1$ nA).

Assuming that all noise sources are uncorrelated, the minimum detectable phase signal is

$$\phi_{\text{smin}} = \left[(\phi_{s\text{Phase}})^2 + (\phi_{s\text{Shot}})^2 + (\phi_{s\text{Electronic}})^2\right]^{1/2}. \quad (18)$$

As Fig. 3 shows, phase noise is dominant. Therefore

$$\phi_{\text{smin}} \approx \phi_{s\text{Phase}} = \sqrt{\frac{16N(N+1)\tau_c}{V^2}}. \quad (19)$$

This expression does not depend on "M"; therefore, from the viewpoint of sensor sensitivity, there is no advantage in using an APD instead of a p-i-n diode.

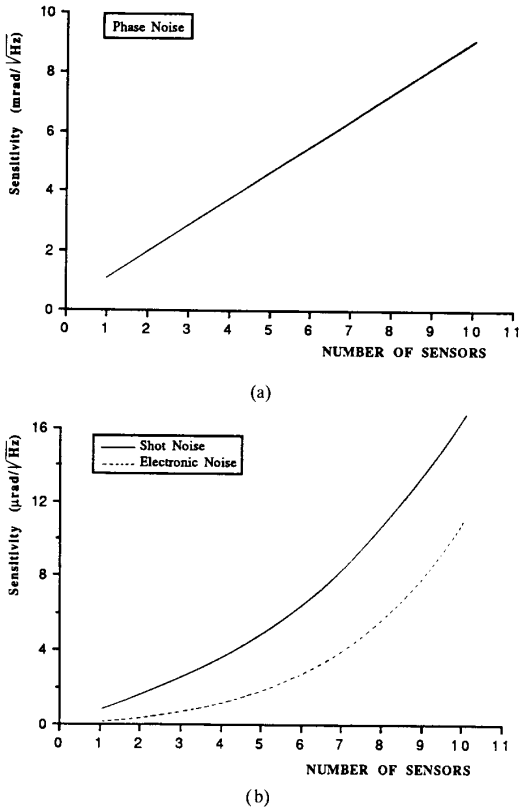

Fig. 3. Variation of the minimum detectable phase signal with the number of sensors, considering: a) only phase noise; b) only shot noise and electronic noise.

C. Reduction of the System Noise Floor

When the pseudo-heterodyne carriers are generated using piezoelectric elements in the reference arms of the interferometers (this does not violate the requirement of electrical passivity in the remote sensing region, because the reference arms can be located together with the laser and its associated drive electronics, the detectores and signal processing electronics), the path imbalance of the interferometers can then be made as small as physically possible. In this case, the level of phase noise can be reduced by modulating the injection current of the laser diode at high frequency [10]. This current modulation also results in modulation of the frequency of the emitted radiation and the output of the jth sensing interferometer becomes (sinusoidal modulation with frequency "ω_m")

$$P_j = P_{\text{int}}[1 + V\cos(\phi_{ms}\sin\omega_m t + \phi_{rj} + \phi_{sj})] \quad (20)$$

where $\phi_{rj} = \omega_{jt}$, $\omega_m >> \omega_j$, and "ϕ_{sj}" is the phase signal applied to the interferometer (constant phases are neglected). If "Δv_m" is the amplitude of the frequency modulation of the source then the induced phase in the interferometer is

$$\phi_{ms} = \frac{2\pi n \Delta L_j \Delta v_m}{c}. \quad (21)$$

The expansion of (20) in terms of Bessel functions gives

$$P_{j|\text{baseband}} = P_{\text{int}} V J_o(\phi_{ms})\cos(\omega_j t + \phi_{sj}). \quad (22)$$

From this expression it can be seen that the laser modulation has the effect of reducing the signal amplitude by the factor "$J_o(\phi_{ms})$." If "ϕ_{ms}" is small the loss in signal strength is negligible. The effect of source modulation on the level of the source induced noise floor can be estimated using a simple model. Let "ΔL_{inc}" be the geometric path imbalance of any two arms in the system not belonging to the same sensing interferometer, i.e., $\Delta L_{\text{inc}} >> \Delta L_c$. The interference of light arriving from these arms gives

$$P_{\text{noise}} = P_{\text{int}} V_{\text{inc}} \cos(\phi_{mn}\sin\omega_m t + \phi_n) \quad (23)$$

where

$$\phi_{mn} = \frac{2\pi n \Delta L_{\text{inc}} \Delta v_m}{c}; \quad \phi_n = \frac{2\pi n \Delta L_{\text{inc}} \delta v}{c} \quad (24)$$

and "ϕ_n" is the phase noise due to fluctuations "δv" of the source frequency and "V_{inc}" is the fringe visibility of the interference of the two "incoherent" beams. Its average value is zero, but not its rms value, because of fluctuations in the source coherence length. Expanding (23)

$$P_{\text{noise|baseband}} = P_{\text{int}} V_{\text{inc}} J_o(\phi_{mn})\cos\phi_n \quad (25)$$

$$P_{\text{noise|}1th-\text{harmonic}} = P_{\text{int}} V_{\text{inc}} J_1(\phi_{mn})\cos[\omega_m t + \phi_n]. \quad (26)$$

Equation (26) indicates that the intensity fluctuations due to fluctuations in "ϕ_n" are distributed around "ω_m" (or $p\omega_m, p = 2, 3, \cdots$, for higher harmonics). If "f_m" ($\omega_m = 2\pi f_m$) is large (MHz region), due to the $1/f$ dependence of the phase fluctuations [11], the noise spectral power in the frequency range of interest for sensing applications is negligible. Therefore, the only noise term that needs to be considered is that given by (25). Compared with the case of zero modulation ($\phi_{mn} = 0, J_o(\phi_{mn}) = 1$) the noise floor will be decreased by a factor

$$F = \frac{1}{J_o(\phi_{mn})}. \quad (27)$$

In practice, the noise floor is limited by the presence of other noise sources. Therefore, it is predicted that "F" will reach a saturation value when "ϕ_{mn}" increases.

D. Crosstalk Analysis

In this section several crosstalk sources will be investigated, namely:

1) some degree of residual interference between light that propagates in distinct sensing interferometers;
2) amplitude modulation of the light emitted by the laser diode when the sensors carriers are generated by ramping the laser diode injection current;
3) the finite fly-back time of the sawtooth waveform (applied to the laser diode or to PZTs used to generate the carriers);
4) driving the phase of the interferometers over noninteger number of fringes in the process of generating the carriers.

The first source of crosstalk is intrinsic to the topology studied; the other three are associated with the practical implementation of the pseudo-heterodyne processing scheme. In this analysis coupled effects between crosstalk mechanisms will not be considered.

1) Crosstalk Due to the Coherence of the Source: This results from the fact that light from a given path is never completely incoherent relatively to light that propagates in the nearest path (worst-case situation). If "L" is the length of fiber that separates two adjacent arms, the level of crosstalk (assuming Lorentzian spectral mode profile) is

$$A_{\text{int}} = 10 \log\left[\exp\left(-\frac{2Ln}{L_c}\right)\right]. \tag{28}$$

For $L = 15$ m and $L_c = 3.6$ m, $A_{\text{int}} = -33$ dB.

2) Crosstalk Due to Amplitude Modulation of the Emitted Light: Fig. 4(a) shows the injection current waveform applied to the laser diode. Its Fourier expansion is

$$i(t) = i_o + \frac{\Delta i}{\pi} \sum_{p=1}^{\infty} \frac{(-1)^{p+1}}{p} \sin(p\omega_r t) \tag{29}$$

where $\omega_r = 2\pi/T$, and "T" is the period of the sawtooth waveform. It is assumed that the path imbalance "ΔL_j" of the jth interferometer is "$m_j \Delta L_{\min}$," where "m_j" is an integer greater than zero and "$\Delta L_{\min}$" is the minimum path imbalance of the set of sensing interferometers. The current excursion that will cause the phase of the interferometer with path imbalance "$\Delta L_{\min}$" to be driven over one fringe is

$$\Delta i = \frac{c}{n\gamma \Delta L_{\min}} \tag{30}$$

where "γ" is the slope of the optical frequency versus injection current curve. The variation "Δi" in the injection current generates a change "$\alpha \Delta i$" in the injected power into the fiber, where "α" is the product of the injection efficiency of optical power into the fiber and the slope of the optical power versus injection current curve in the region above threshold. Assuming zero fly-back time of the sawtooth waveform, the output of the jth interferometer is

$$P_j = u[P_{\text{in}} + \alpha i(t)][1 + V \cos(m_j \omega_r t)] \tag{31}$$

where $u = P_{\text{int}}/P_{\text{in}}$ (the signal applied to the sensor arm is not made explicit in (31)). In this expression the relevant term is

$$uV\alpha i(t) \cos(m_j \omega_r t) = \frac{u\alpha V \Delta i}{2\pi} \sum_{p=1}^{\infty} \frac{(-1)^{p+1}}{p} \cdot \left[\sin[(p - m_j)\omega_r t] + \sin[(p + m_j)\omega_r t]\right]. \tag{32}$$

We can consider now the crosstalk from the jth sensor to the j'th sensor, whose carrier frequency is $\omega_{j'} = (m_j + p)\omega_r$ (or $(m_j - p)\omega_r$). From (31) and (32)

$$P_{j'}[\omega_{j'} = (m_j + p)\omega_r] \approx uP_{\text{in}}V$$
$$P_j[\omega = \omega_{j'} = (m_j + p)\omega_r] \approx \frac{u\alpha V \Delta i}{2\pi p}. \tag{33}$$

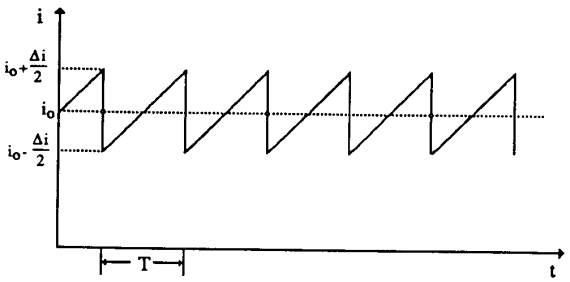

(a)

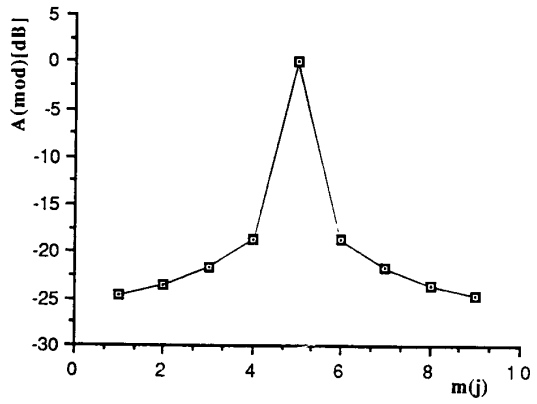

(b)

Fig. 4. a) Injection current waveform applied to the laser diode. b) Crosstalk from the jth sensor (with $\omega_j = 5\omega_r$) to other harmonics due to the amplitude modulation of the emitted light ($p = |m_j - m_{j'}|$).

Therefore, the amount of crosstalk from sensor j to sensor j' due to the amplitude modulation of the laser diode emitted light is

$$A_{\text{mod}_{|j->j'}} \equiv 10 \log\left[\frac{P_j(\omega = \omega_{j'})}{P_{j'}}\right] = 10 \log\left[\frac{\alpha c}{2\pi p n \gamma P_{\text{in}} \Delta L_{\min}}\right]. \tag{34}$$

For a given system configuration the crosstalk is maximum when $p = 1(|\omega_j - \omega_{j'}| = \omega_r)$. Fig. 4(b) shows "$A_{\text{mod}}$" when $m_j = 5$ and: $\gamma = 3$ GHz/mA, $\alpha = 0.13$ mW/mA (typical values for the HL7801 laser diode, and considering a power injection efficiency into the fiber of 30%), $P_{\text{in}} = 1$ mW and $\Delta L_{\min} = 10$ cm.

3) Crosstalk Due to the Finite Fly-back Time of the Sawtooth Waveform: This effect is illustrated in Fig. 5 for the case $m_j = 2$. From this figure

$$T_r = \mu T \qquad T_f = (1 - \mu)T; \qquad 0 < \mu \leq 1. \tag{35}$$

The output from the jth interferometer is (AC component)

$$P_{j|AC} = P_{\text{int}} v_{\cos}\left[\frac{2\pi m_j}{\mu T} t\right]; \quad 0 \leq t < \mu T$$
$$= P_{\text{int}} v_{\cos}\left[\frac{2\pi m_j}{(1 - \mu)T}(T - t)\right]; \quad \mu T \leq t \leq T. \tag{36}$$

This function is periodic with period "T"; therefore, it can be expanded in a Fourier series

$$P_{j|AC} = P_{\text{int}} V \sum_{p=1}^{\infty} \Big[A_p \cos(p\omega_r t) + B_p \sin(p\omega_r t) \Big]$$
$$= P_{\text{int}} V \sum_{p=1}^{\infty} S_p \cos(p\omega_r t + \alpha_p) \tag{37}$$

where $w_r = \frac{2\pi}{T}$ and

$$S_p = \Big[A_p^2 + B_p^2 \Big]^{1/2}. \tag{38}$$

The expansion coefficients are given by

$$A_p = \frac{1}{T} \Bigg\{ \frac{\sin[(a - p\omega_r)\mu T]}{a - p\omega_r} + \frac{\sin[(a + p\omega_r)\mu T]}{a + p\omega_r}$$
$$+ \frac{1}{p\omega_r - b} \Big[\sin[d + (p\omega_r - b)T] - \sin[d + (p\omega_r - b)\mu T] \Big]$$
$$+ \frac{1}{p\omega_r + b} \Big[\sin[(p\omega_r + b)T - d] - \sin[(p\omega_r + b)\mu T - d] \Big] \Bigg\};$$
$$p = 0, 1, 2, \cdots \tag{39}$$

$$B_p = \frac{1}{T} \Bigg\{ \frac{1}{p\omega_r - a} \Big[1 - \cos[(p\omega_r - a)\mu T] \Big]$$
$$+ \frac{1}{p\omega_r + a} \Big[1 - \cos[(p\omega_r + a)\mu T] \Big]$$
$$+ \frac{1}{p\omega_r - b} \Big[\cos[d + (p\omega_r - b)\mu T]$$
$$- \cos[d + (p\omega_r - b)T] \Big] + \frac{1}{p\omega_r + b}$$
$$\cdot \Big[\cos[(p\omega_r + b)\mu T - d] - \cos[(p\omega_r + b)T - d] \Big] \Bigg\};$$
$$p = 1, 2, 3, \cdots \tag{40}$$

where

$$a = \frac{2\pi m_j}{\mu T}; \qquad b = \frac{2\pi m_j}{(1 - \mu)T}; \qquad d = \frac{2\pi m_j}{1 - \mu}. \tag{41}$$

When $\mu = 1$ (zero fly-back time) $B_p = 0$ and $A_p = 0$ for all "p", except where $p = m_j$, when $A_{m_j} = 1$. This means that the optical energy is all concentrated in the frequency $\omega_j = m_j \omega_r$. When $\mu < 1$, $A_{m_j} < 1$ and the energy is spread over the other harmonics, generating crosstalk from the jth sensor to sensors with carriers $\omega_{j\prime}$, $m_{j\prime} \neq m_j$. This crosstalk can be measured by the parameter "A_{fly}", defined as

$$A_{\text{fly}|j->j'} \equiv 10 \log \left[\frac{P_j(\omega = \omega_{j'})}{P_{j'}} \right] = 10 \log [S_p] \tag{42}$$

where $P_j(\omega = \omega_{j'})$ is the optical power of the jth interferometer in the carrier frequency of interferometer "j'", "$P_{j'}$" is the optical power of interferometer "j'" in its carrier frequency, and $p = m_{j'}$. Fig. 6 gives "A_{fly}" for the case $1/T = 1$ kHz, $m_j = 5$ and $\mu = 0.98$ (this value corresponds to a fly-back time of 20 μs). As could be expected, crosstalk energy appears essentially at frequencies greater than "ω_j".

4) Crosstalk Due to Phase Modulation over a Noninteger Number of Fringes: The effect is illustrated in Fig. 7. The

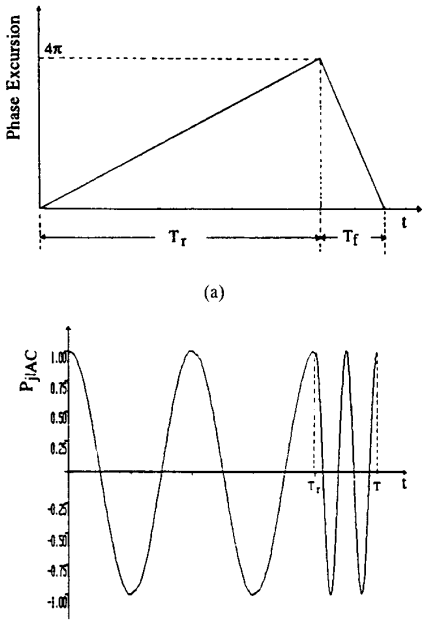

Fig. 5. a) Phase waveform applied to the interferometer for modulation over two fringes. b) Corresponding interferometer output (AC component; $P_{\text{int}} V = 1$.)

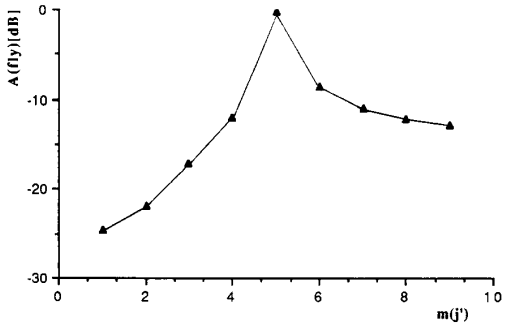

Fig. 6. Crosstalk from the jth sensor (with $m_j = 5$) to other harmonics due to the finite fly-back time of the sawtooth waveform ($\mu = 0.98$; $p = m_{j'}$).

output from the jth interferometer (AC component) is

$$P_{j|AC} = P_{\text{int}} V \cos \Big[\frac{2\pi m_j \varepsilon}{T} t \Big]; \quad 0 \leq t \leq T \tag{43}$$

where the parameter "ε" models the deviation from the phase modulation over an integer (m_j) number of fringes. Again, because this function repeats itself with period "T," it can be expanded in the Fourier series given by (37), with coefficients

$$A'_p = \frac{1}{2\pi} \left[\frac{\sin[2\pi(m_j\varepsilon - p)]}{m_j\varepsilon - p} + \frac{\sin[2\pi(m_j\varepsilon + p)]}{m_j\varepsilon + p} \right];$$
$$p = 0, 1, 2, \cdots \tag{44}$$

$$B'_p = \frac{1}{2\pi} \left[\frac{\cos[2\pi(m_j\varepsilon - p)]}{m_j\varepsilon - p} - \frac{\cos[2\pi(m_j\varepsilon + p)]}{m_j\varepsilon + p} \right.$$
$$\left. - \frac{1}{m_j\varepsilon - p} + \frac{1}{m_j\varepsilon + p} \right]; \qquad p = 1, 2, 3, \cdots. \tag{45}$$

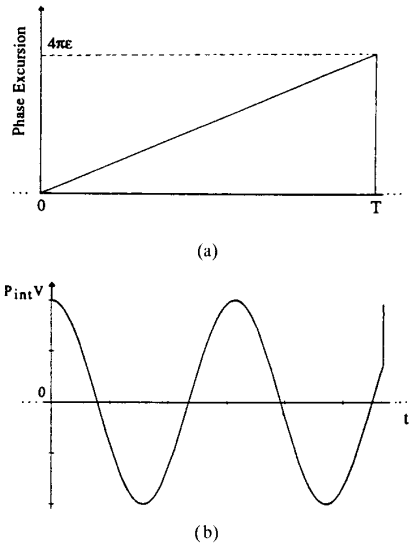

Fig. 7. a) Phase waveform applied to the interferometer for modulation over 2ε fringes ($\varepsilon = 0.9$); b) interferometer output (AC component).

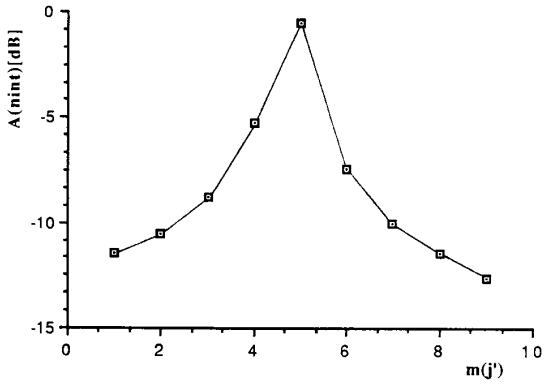

Fig. 8. Crosstalk from the jth sensor ($m_j = 5$) to other harmonics due to modulation over a noninteger number of fringes ($\varepsilon = 0.95$; $p = m_{j'}$).

When $\varepsilon = 1$ (phase modulation over an integer number of fringes), $B'_p = 0$ and $A'_p = 0$ for all "p," except when $p = m_j$, where $A'_{m_j=1}$. Therefore, the optical energy is totally concentrated in the frequency $\omega_j = m_j\omega_r$. When $\varepsilon \neq 1$, the energy is spread over other harmonics causing crosstalk from the jth sensor to sensors with carriers $\omega_{j'}$, $m_{j'} \neq m_j$. This crosstalk can be measured by the parameter "A_{nint}", defined as

$$A_{\text{nint}|_{j->j'}} \equiv 10\log\left[\frac{P_j(\omega = \omega_{j'})}{P_{j'}}\right] = 10\log\left[S'_p\right] \quad (46)$$

where $p = m_{j'}$ and

$$S'_p = \left[A'^2_p + B'^2_p\right]^{1/2}. \quad (47)$$

Fig. 8 gives "A_{nint}" for the case $m_j = 5$ and $\varepsilon = 0.95$ (one quarter of a fringe is missing).

E. Lead Insensitivity

The multiplexing topology shown in Fig. 1 can be made insensitive to phase fluctuations induced in the fiber leads by external agents using active compensation. Referring back to Fig. 1, the output from the jth interferometer can be written as

$$P_j = P_{\text{int}}[1 + V\cos(\phi_{rj} - \phi_{sj} + \phi_c - \phi_d)] \quad (48)$$

where $\phi_{rj} = \omega_j t$, "ϕ_{sj}" is the applied phase signal, "ϕ_d" is the environmentally induced phase fluctuation and "ϕ_c" is the phase introduced by the compensating servo system. When this system is operating "$\phi_c - \phi_d$" is kept constant within the servo bandwidth, thereby eliminating the phase fluctuations. Because the input to the servo is obtained from the amplifier output after low-pass filtering, the minimum carrier frequency must be larger than the servo bandwidth. However, no constraint is imposed on the frequency of the applied signals.

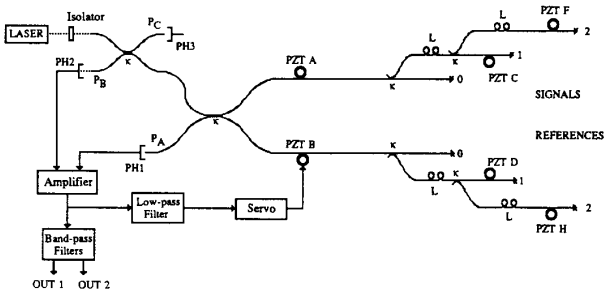

Fig. 9. Experimental arrangement (the nominal value for the coupling constant "κ" is 0.5).

III. EXPERIMENT

The multiplexed network concept discussed above was tested for $N = 2$. Fig. 9 shows the experimental arrangement. The optical source used was a laser diode Hitachi 7801E. For an emitted light power of 2.5 mW the power injected into the fiber was 250 μW. All couplers had nominal 50/50 coupling ratios. The ends of the fibres of each of the three interferometers were silvered. The interferometers arms were separated by fibers with a length "L" of 19 m. Signals were induced in the interferometers using PZT's (interferometer "0": PZT A, B; interferometer "1": PZT C, D; interferometer "2": PZT F, H). The detectors were p-i-n diodes. Dual detection was implemented using outputs A and B[1]. The signal from the output of the differential amplifier was bandpass filtered to provide the carriers for interferometers "1" and "2." In addition, the amplifier output (after low-pass filtering) was applied to a servo which generates an error signal to maintain interferometer "0" in quadrature, thereby compensating any fluctuations induced in the fiber leads.

The losses in the fiber, splices and couplers, when lumped together as an equivalent total loss located in the couplers, gave $\beta = 0.8$. The power "p_o" (output A) returned from each arm of interferometer "0" was 2.3 μW; the power returned from each of the arms of interferometers "1" and "2" was

[1] When phase noise is the dominant noise source dual detection will improve the system sensitivity by a factor of $\sqrt{2}$, i.e., $\phi_{\text{s min}\,A} = \phi_{\text{s min}\,B} = \sqrt{2}\phi_{\text{s min Dual}}$.

$p_1 \approx p_2 \approx 0.4$ μW. The modulation efficiencies of the PZT's were evaluated as being: A: 0.63 rad/V; B: 1.74 rad/V; C: 0.31 rad/V; D: 0.75 rad/V; F: 0.28 rad/V; H: 0.9 rad/V. The dynamic range of the servo system was 163 rad and the 3-dB cutoff frequency was 400 Hz.

The visibility for any of the three inteferometers is not directly accessible from outputs "A" or "B," because these give the sum of the optical powers arriving from the interferometers. However, if for interferometer "i" ($i = 0, 1, 2$) the measured visibility "V_{ia}" is obtained in the usual way, the true visibility is

$$V_i = \frac{p_o + p_1 + p_2}{P_i} V_{ai}. \tag{49}$$

Using this expression, the calculated visibilities were: $V_o \approx 43\%$, $V_1 \approx V_2 \approx 38\%$. The geometric path imbalances of interferometers "0," "1" and "2" were $2 \times (0.8 \pm 0.1)$ cm, $2 \times (7.5 \pm 0.3)$ cm, and $2 \times (15 \pm 0.3)$ cm, respectively, equivalent to OPD's of 2.3 ± 0.3 cm, 22 ± 0.9 cm, and 44 ± 0.9 cm, respectively.

IV. Results

Fig. 10 shows the output of the amplifier when a sinusoidal test signal of amplitude "V_s" (frequency: 1 kHz) was applied to interferometer "0" (via PZT A). Fig. 10(a) was obtained when only interferometer "0" was present and $V_s = 8$ mV; Fig. 10(b) is for the case when interferometers "0" and "1" were present and $V_s = 20$ mV; finally, Fig. 10(c) respects to all the system being connected and $V_s = 20$ mV. The sensitivity obtained for each of the three cases is 14 $\mu\text{rad}/\sqrt{\text{Hz}}$, 141 $\mu\text{rad}/\sqrt{\text{Hz}}$, and 221 $\mu\text{rad}/\sqrt{\text{Hz}}$, respectively.

The lead insensitivity is illustrated in Fig. 11. A sawtooth waveform (frequency: 2 kHz) with appropriate amplitude was applied to one of the arms of interferometer "1" (via PZT D) in order to drive the interferometer phase over 2π radians (one fringe) and generate a pseudo-heterodyne carrier. A small sinusoidal signal (frequency: 100 Hz) was applied to PZT A, to simulate the environmental noise on the transceiver lead. Fig. 11(a) is the output of the system when the servo was off. As expected, the noise signal also appears as sidebands of the carrier, and would be interpreted as a signal detected by interferometer "1". When the servo loop was closed (Fig. 11(b)) the induced signal was attenuated by 32 dB and no sidebands appeared in the carrier, demonstrating the lead insensitivity of this configuration.

Fig. 12 shows the carriers generated in interferometer "1" (frequency: 2.5 kHz) and interferometer "2" (frequency: 5 kHz) when sawtooth waveforms were applied to PZT's D and H, respectively, with an amplitude selected to modulate the phase of the interferometers over one fringe (the electronic sawtooth waveforms had fly-back times of 5 μs; the PZT's used had cutoff frequencies around 80 kHz, which implies PZT fly-back times of the order of 15 μs). In Fig. 12(a) a test signal (frequency: 250 Hz; amplitude: 123 mrad) was applied to interferometer "1" (via PZT C) and no signal was applied to interferometer "2"; in Fig. 12(b) the same signal was applied to interferometer "2" (via PZT F) and no signal was applied to interferometer "1". As can be seen, no sideband crosstalk is

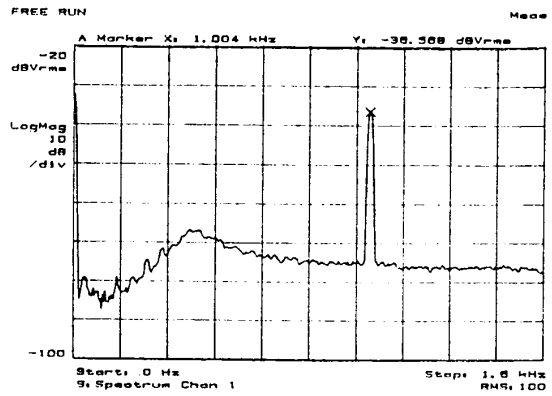

(a)

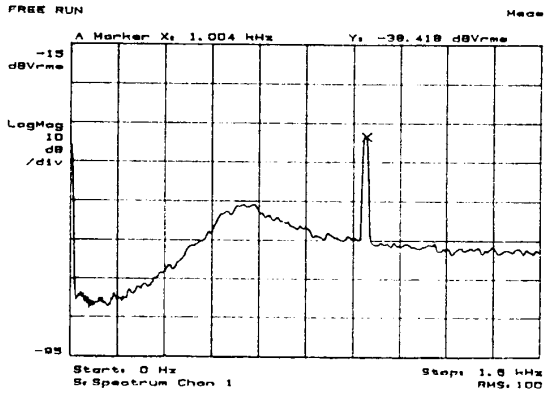

(b)

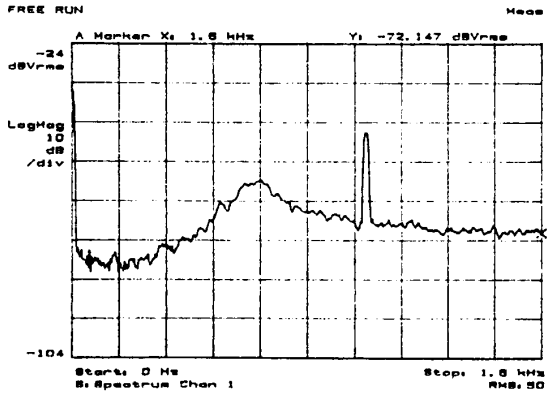

(c)

Fig. 10. Output of the system when a test signal was applied to interferometer "0" (B = 16 Hz): a) only interferometer "0"; b) interferometers "0" + "1"; c) interferometers "0" + "1" + "2".

apparent between the two sensors. For the situation described, the main source of crosstalk is the finite fly-back time of the sawtooth waveforms. From the theory presented in Section II-D.3 we find $A_{\text{fly}|1->2} = -24$ dB and $A_{\text{fly}|2->1} = -28$ dB (defined as $20 \log(P_j/P_{j'})$). These values clearly indicate that the crosstalk signals are below the noise floor. From the data presented, the sensitivity of the sensors was estimated to be 5 mrad/$\sqrt{\text{Hz}}$.

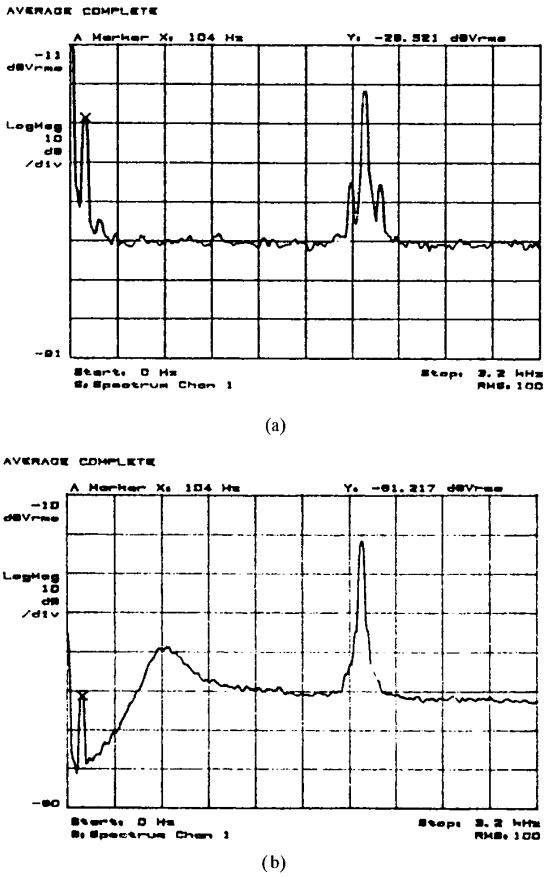

Fig. 11. Effect of the compensating scheme (carrier generated in interferometer "1"; lead signal applied to interferometer "0"): a) servo off; b) servo on.

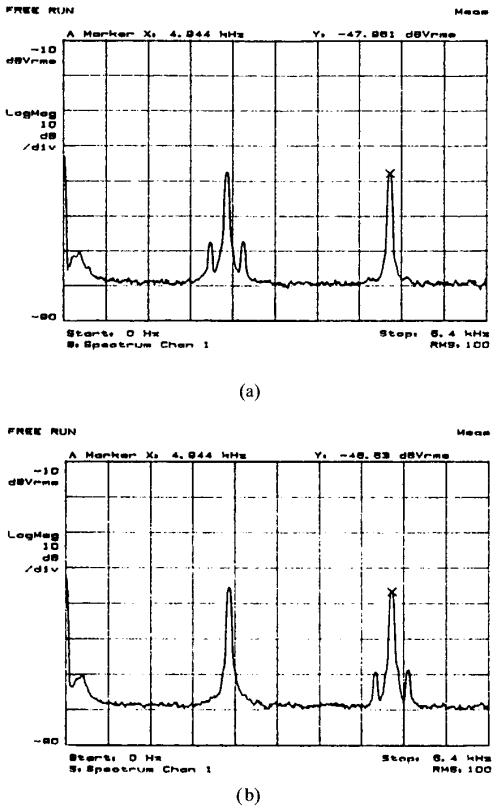

Fig. 12. Interferometers carriers and test signals (B = 64 Hz); a) test signal applied to interferometer "1"; b) test signal applied to interferometer "2".

Similar results to those shown in Fig. 12 were obtained when the carriers of the interferometers were generated by modulating the injection current of the laser diode with a sawtooth waveform (frequency: 2.5 kHz) with amplitude adjusted to modulate the phase of interferometer "1" over one fringe, which gives a modulation for the phase of interferometer "2" over approximately 2 fringes (the path imbalance of this interferometer was twice that of interferometer "1").

Further experiments were performed with this system to test the concept of noise reduction via high frequency laser diode modulation. The carriers were now generated by modulation of PZT's D and H. A sinusoidal waveform (frequency: 2 MHz) was applied to the laser diode, with a peak-to-peak current excursion of 7.9 mA. The slope "γ" of the optical frequency versus injection current curve was measured as being 0.48 GHz/mA at 2 MHz. Therefore, the current excursion gave a frequency sweep of 3.8 GHz. A test signal was applied to interferometer "0" via PZT A (frequency: 3 kHz, amplitude: 20 mV). The results are shown in Fig. 13 (a). When the modulation is off, $S/N \approx 17$ dB, which gives a sensitivity of 220 μrad/$\sqrt{\text{Hz}}$. When the modulation is on, the noise floor is decreased by 18 dB while the signal amplitude was reduced by 2.5 dB (from (21) and (22), the theoretical value for the amplitude reduction is 2.2 dB). Therefore, $S/N \approx 32$ dB, which results in a sensitivity of 37 μrad/$\sqrt{\text{Hz}}$ (similar reduction in the noise level was obtained when square or triangular waveforms were used, instead of a sinusoidal modulation).

The dependence of the factor of reduction "F" of the level of the system noise floor with the amplitude of the applied modulation current is given in Fig. 13(b). "F" increases with the increase of the amplitude of the modulation current, approaching a saturation value of approximately 10. This value is set by the presence of other noise sources (shot and electronic noise), which become comparable to the residual level of phase noise present in the baseband.

V. Discussion

The experimental values for the sensitivity of interferometer "0", obtained from Fig. 10, can be compared with those derived from the expressions presented in Section II-B, taking into account that, for this particular case, homodyne processing is used (the signal strength is doubled as compared with the pseudo-heterodyne processing). The theoretical values are: 8 μrad/$\sqrt{\text{Hz}}$ when only interferometer "0" is present; 171 μrad/$\sqrt{\text{Hz}}$ (interferometers "0" + "1"); 256 μrad/$\sqrt{\text{Hz}}$ (interferometers "0" + "1" + "2"). For the first case, electronic

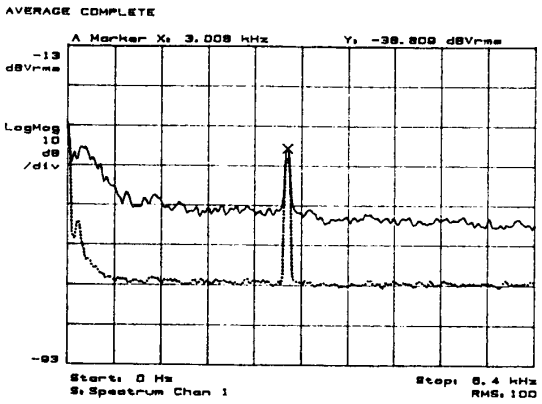

(a)

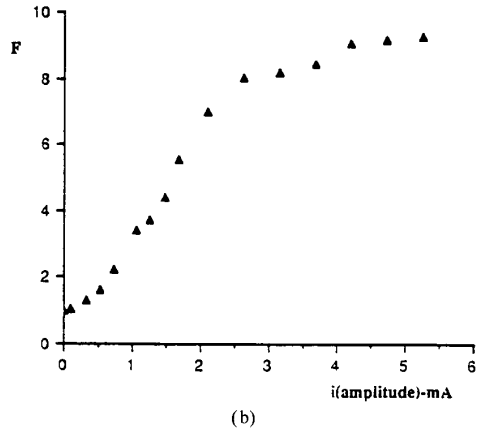

(b)

Fig. 13. a) Effect of the laser diode modulation (dotted line: modulation on; $B = 64$ Hz); b) Variation of the system noise floor reduction factor with the amplitude of the modulation current.

noise is the dominant noise source (particularly, amplifier noise from the 741 amplifier: $i_n = 4 \times 10^{-12}$ pA/$\sqrt{\text{Hz}}$). For the other two cases, phase noise was clearly the dominant noise source and the sensitivity values were obtained from an estimated source coherence length of 2.4 m. The calculated values are close to those obtained experimentally. However, when phase noise is dominant, the theoretical values are worse than the experimental ones. This can be understood by the fact that the model used in [7] to obtain the phase noise power spectral density assumes a constant polarization state across the optical system. In practice, some degree of polarization mismatch in the output beams is inevitable, with the consequence that the actual "$G_{\text{PhaseNoise}}$" is smaller than the value given by (6) (the effect of this polarization mismatch on the signal level has already been taken into account by the measured value of the fringe visibility).

The phase sensitivity of interferometers "1" and "2," multiplexed in frequency and using pseudo-heterodyne processing, was found to be 5 mrad/$\sqrt{\text{Hz}}$. From (17), with $P_{\text{int}} = 2p_1 = 2p_2 \approx 0.8$ μW, the theoretical sensitivity is 3.5 mrad/$\sqrt{\text{Hz}}$. The agreement between the two values is reasonable if we consider that the finite fly-back time of the PZT's has the effect of spreading energy into other harmonics of the sawtooth frequency (Fig. 6), decreasing the sensor sensitivity. One way to improve the sensitivity is to increase powers "p_1" and "p_2" by optimizing the system. If the coupling ratios of the couplers were given by (5b), with $\beta = 0.8$ we would have $\kappa_o = 0.5$, $\kappa_1 = 0.71$, $\kappa_2 = 0.5$ and $p_1 \approx p_2 \approx 0.8$ μW, giving a theoretical sensitivity of 1.5 mrad/$\sqrt{\text{Hz}}$. Another method would be to reduce the system noise floor by applying high frequency modulation to the laser diode. Fig. 13(a) indicates a noise level reduction of 18 dB. If the carriers are generated via PZT's applied to the reference arms of the interferometers (which is feasible with the present topology) then the path imbalance of the interferometers could be made as small as possible, resulting in a negligible loss in signal strength due to the modulation. Therefore, the measured reduction of the noise floor would give a sensor sensitivity of 0.6 mrad/$\sqrt{\text{Hz}}$.

The results obtained show that the sensitivity achieved with frequency multiplexing is relatively poor. This is due to the presence of multiple paths in the network, with large path imbalances, in combination with the use of sources with large coherence length (single-mode laser diodes). This combination introduces large levels of source induced noise in the output of the system. When a particular topology is amenable to carrier generation using PZT's, alternative light sources with much smaller coherence length (for example, superluminescent diodes or multimode laser diodes) could be used, which would provide substantially lower levels of source induced noise, with the corresponding improvement in sensor sensitivity.

The analysis of crosstalk given in Sections II-D.2–II-D.4 is general and can be applied to any frequency multiplexing scheme based on carrier generation using sawtooth waveforms applied to PZT's or to the injection current of laser diodes. When PZT's are used, the main crosstalk source is the sawtooth fly-back time. PZT's act as low-pass filters with relatively low cutoff frequency (typically some tens of kilohertz). Consequently, the PZT's fly-back time can be long, resulting in an increase on the crosstalk levels (this effect can be avoided using sinusoidal modulation with appropriate gating of the output signals [12]). When the carriers are generated using laser diode frequency modulation, the main crosstalk source will be the phase modulation over a noninteger number of fringes. Frequency multiplexing with laser diode modulation implies that the path imbalances of the sensing interferometers must be integer multiples of a minimum path imbalance "$\Delta L_{\min}$." In practice, this condition is difficult to fulfill exactly, with the consequent increase of sensor crosstalk (nonlinearities in the ramped phase of the interferometer will also introduce extra crosstalk between sensors [13]).

In conclusion, a scheme to frequency multiplex a group of sensors based on all fiber Michelson interferometers was presented. Lead insensitivity was obtained using active compensation. Topics concerning system design, sensor sensitivity and crosstalk levels were investigated. The concept was demonstrated with two sensors and the results compared with those derived from the model developed.

REFERENCES

[1] D. A. Jackson and J. D. C. Jones, "Optical fibre sensors," *Optica Acta,* vol. 33, p. 1469, 1986.

[2] J. P. Dakin, "Multiplexed and distributed optical fibre sensors," *J. Phys. E: Sci. Instru.* vol. 20, p. 954, 1987.

[3] B. Culshaw, "Distributed and multiplexed fibre optic sensor systems," *NATO ASI Series, E.* no. 132, p. 165, 1987.

[4] P. G. Cielo, "Fiber optic hydrophone: Improved strain configuration and environmental noise," *Appl. Opt.,* vol. 18, p. 2933, 1979.

[5] S. W. Thornton, M. L. Henning, and R. J. Langston, "Experimental performance of an optical hydrophone," *2nd Internat. Conf. Optical Fibre Sensors* (The Hague), Sept. 1984, p. 369.

[6] D. T. Jong and K. Hotate, "Optical fibre interferometer sensor with immunity from environmental disturbance induced in the lead fibre," *6nd Internat. Conf. Optical Fibre Sensors,* Paris, Sept. 1989, p. 313.

[7] B. Moslehi, "Noise power spectra of optical two-beam interferometers induced by the laser phase noise," *J. Lightwave Technol.,* vol. 4, p. 1704, 1986.

[8] R. H. Wentworth, "Theoretical noise performance of coherence multiplexed interferometric sensors," *J. Lightwave Technol.,* vol. 7, p. 941, 1989.

[9] R. C. Youngquist, "Coherence length and output power of GaAlAs single mode laser diodes: A rule of thumb relationship," *Appl. Opt.,* vol. 24, p. 1400, 1985.

[10] A. Kersey and A. Dandridge, "Phase-noise reduction in coherence-multiplexed interferometric fibre sensors," *Electron. Lett.,* vol. 22, p. 616, 1986.

[11] A. D. Kersey, D. A. Jackson, and M. Corke, "A simple fibre Fabry–Perot sensor," in *Proc. Internat. Conf. Opt. Tech. Process Control* (The Hague); B1, 1983.

[12] A. C. Lewin, A. D. Kersey, and D. A. Jackson, "Non-contact surface vibration analysis using a monomode fibre optic interferometer incorporating an open air path," *J. Phys. E: Sci. Instru.,* vol. 18, p. 604, 1985.

[13] G. Economou, R. C. Youngquist, and D. E. N. Davies, "Limitations and noise in interferometric systems using frequency ramped single mode diode lasers," *J. Lightwave Technol.,* vol. LT-4, p. 1601, 1986.

J. L. Santos, photograph and biography not available at the time of publication.

F. Farahi, photograph and biography not available at the time of publication.

T. Newson, photograph and biography not available at the time of publication.

A. P. Leite, photograph and biography not available at the time of publication.

D. A. Jackson, photograph and biography not available at the time of publication.